I&EC research
Industrial & Engineering Chemistry Research

Article

pubs.acs.org/IECR

Functionalized Graphene from Electrochemical Exfoliation for Thermoplastic Polyurethane: Thermal Stability, Mechanical Properties, and Flame Retardancy

Wei Cai,[†] Xiaming Feng,[†] Weizhao Hu,[†] Ying Pan,[†] Yuan Hu,[*,†] and Xinglong Gong[*,‡]

[†]State Key Laboratory of Fire Science, University of Science and Technology of China, Anhui 230026, PR China

[‡]CAS Key Laboratory of Mechanical Behavior and Design of Materials, Department of Modern Mechanics, University of Science and Technology of China, Hefei, Anhui 230026, PR China

ABSTRACT: Mass production of graphene was successfully achieved with a simple and environmentally friendly electrochemical exfoliation approach. The obtained graphene was noncovalently modified by ligninsulfonate and iron ion (Fe-lignin) to form the flame retardant functionalized graphene sheets (FGNS). Subsequently, FGNS was introduced to reduce fire hazards of thermoplastic polyurethane (TPU). The FGNS/TPU nanocomposites presented higher thermal conductivity, thermal stability, and flame retardancy than those of neat TPU. By adding 2.0 wt% FGNS, a significant reduction (62.8%) in peak heat release rate (pHRR) and high char yield (from 3.6 to 9.4 wt %) were observed. During the combustion, in situ formed char derived from catalysis action of Fe-lignin can protect the layer structure of graphene to further hinder the transfer of pyrolysis volatile with barrier effect. The simple exfoliation and effective functionalization of graphene shows a promising application prospect in polymer nanocomposites.

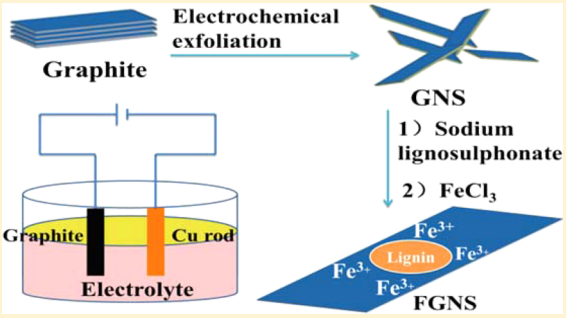

1. INTRODUCTION

Graphene is rapidly developed in many applications, such as electronic devices,[1] sensors,[2] catalysts,[3] and flame retardants.[4] At present, there are three primary approaches to prepare graphene: (i) chemical exfoliation of graphite, (ii) direct exfoliation by shear force or ultrasonic in polar solvent, and (iii) electrochemical exfoliation of graphite. Quite a number of reports in regard to graphene use the graphite oxide means, due to high yield and abundant organo-functional groups. Wang et al. simultaneously modified and reduced graphene oxide with POSS for endowing high fire safety to epoxy composites. In addition, direct exfoliation in liquid phase is also accepted because it can obtain high quality graphene sheet. Aneja et al.[5] fabricated graphene based anticorrosive coatings through high shear liquid exfoliation route and prominently increased the corrosion resistance. However, it is not negligible that inevitable drawbacks exist in the aforementioned two routes. Although the graphite oxide route can provide high yield of graphene sheet, the structure and lattice of graphene are inevitably destroyed in the rigorous oxidation process.[6] On the other hand, direct exfoliation in solution gets high quality graphene sheet at the cost of low output. Only simultaneously meeting the demands of high yield and low defect, graphene can be extensively applied in industrial fields. Compared to the first two approaches, electrochemical exfoliation can acquire large quantities of graphene sheets (a high yield >85%) and a higher quality (a C/O ratio of 17.2) than those of reduced graphene oxide (RGO) in carbon lattice and structural perfection.[7] Furthermore, electrochemical exfoliation avoids the consumption of hazardous chemicals and the reduction process, which is more environmentally friendly than that of chemical exfoliation of graphite. Recently, electrochemically exfoliated graphene had been applied in many fields, such as transparent conductive films[8] and high-rate energy storage,[9] metal-free catalysts,[10] and flexible supercapacitors.[7] But for the moment, electrochemically exfoliated graphene is rarely reported in the application of polymer nanocomposites. This article first employs electrochemistry exfoliated graphene to improve the flame retardancy of TPU.

Thermoplastic polyurethane (TPU) as a kind of elastomer has been widely used in coating,[11] adhesives,[12] and composites.[13] Xiang et al.[12] reported that polyurethane used as the interlayer can effectively bound the carbon materials to the Kevlar fiber with a durable conductivity. Amir et al.[14] prepared graphene based polyurethane resin fibers by a pressurized gyration process, and opened a new approach to produce graphene reinforced composite fibers. However, the application of TPU is remarkably hindered because of its high flammability. Therefore, it is crucial to enhance the flame retardancy of TPU and simultaneously maintain its high mechanical property. In previous literatures, nanofiller has been applied to improve the various performances of polymer, such as CNT,[15] metal oxides,[16] and so on.[17] However, nanofiller

Received: July 6, 2016
Revised: September 13, 2016
Accepted: September 16, 2016
Published: September 16, 2016

DOI: 10.1021/acs.iecr.6b02579
Ind. Eng. Chem. Res. 2016, 55, 10681−10689

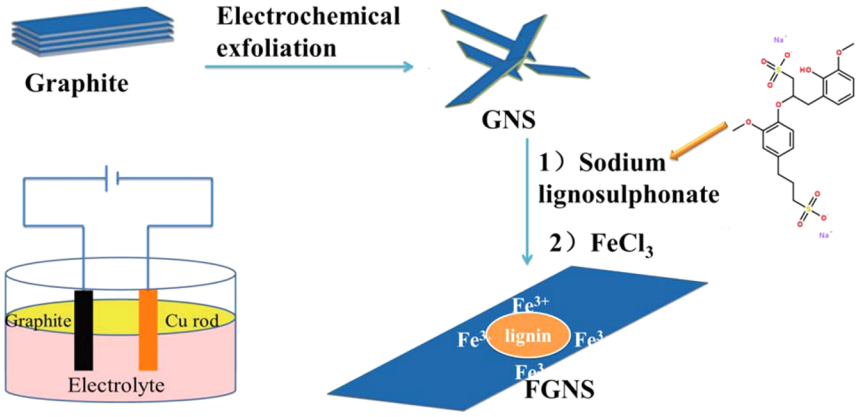

Figure 1. Illustration for electrochemical exfoliation of graphite and the functionalization process.

usually play a synergistic role in flame retardant system for polymer composites due to itself distinction. Unlike above nanofiller, two-dimensional materials have presented a significant impact on the fire safety and the mechanical properties of polymer.[17,18] For example, reduced graphene oxide can obviously inhibit the combustion of polymer, due to the physical barrier effect.[19] Only by maintaining the lamellar morphology, can graphene take full advantage of the shield effect in the combustion process of polymer. However, the layer structure of RGO is easily damaged during the burning process. To overcome this limitation, Feng et al.[20] employed chitosan to simultaneously reduce and modify the graphene oxide (GO); the char derived from chitosan covered on graphene sheets can form a protective char layer to improve the flame retardancy of poly(vinyl alcohol). Bao et al.[21] functionalized GO with char-catalyzing agents, which could improve char formation to maintain the stratified structure of nanofillers. However, a lot of waste of chemical reagent and a tricky step are fatal flaws for chemical exfoliation in the popularization of graphene for practical application. Stemming from the consideration of environmental protection and simple process, electrochemical exfoliation is an alternative way to provide a good future view for the application of graphene.

In this work, we obtained a high quality and low defect graphene by an environmentally friendly electrochemical exfoliation route. The iron lignosulfonate with high char yield was employed to surface modify the graphene in a noncovalent way and protect the lamellar structure from falling apart. Then functionalized graphene was added into TPU matrix by a combination of co-coagulation and the compression molding technique. The effect of functionalized graphene on flame retardancy, mechanical performance, and thermal conductivity of TPU was investigated.

2. EXPERIMENTAL SECTION

2.1. Materials. Graphite piece (purity ≥99%) was purchased from Xinda Material Co., Ltd., China. Sodium sulfate (Na_2SO_4, AP), iron chloride ($FeCl_3$, AP), and *N*,*N*-dimethylformamide (DMF, AP) were offered by Sinopharm Chemical Reagent Co., Ltd., China. Sodium ligninsulfonate was obtained from Xiya Chemical Reagent Corp without further purification. Thermoplastic polyester polyurethane (TPU) was provided by Bangtai Material Co., Ltd., China.

2.2. Electrochemical Preparation of Graphene. The electrochemical exfoliation process was operated in a two-electrode configuration which a sustained and steady potential (~10 V) was carried out. The graphite slice (2.0 cm × 3.0 cm × 0.3 mm) and a copper rod were used as working and counter electrodes, respectively, and were immersed in an electrolyte. The electrolyte for the exfoliation was prepared by dissolving Na_2SO_4 (0.05 mol) in deionized water (100 mL) with 500 mL beaker. The distance of separated electrodes was kept at 1 cm and parallel during the electrochemical preparation process, moreover the temperature was kept at 0 °C. After 4 h, the solution was centrifuged for 10 min at 1500 rpm to separate the unexfoliated graphite. Then the exfoliated graphene sheets (GNS) were collected through vacuum filtration and thoroughly washed with deionized water. Finally, the filter cake was dried in an oven at 80 °C for 24 h to remove the excess water.

2.3. Preparation of Functionalized Graphene. Sodium ligninsulfonate (10.0 g) was dissolved in deionized water (500 mL) in a 1000 mL three-necked flask equipped with a mechanical stirrer. GNS (1.75 g) was dispersed in deionized water (400 mL) with assistance of vigorous stir and ultrasound for 2 h. Then the homogeneous suspension of GNS was slowly added into the sodium ligninsulfonate solution and stirred for 6 h to ensure the noncovalent adsorption. The obtained suspension was thoroughly washed with deionized water by vacuum filtration to remove the needless sodium ligninsulfonate. Afterward, the modified graphene (L-GNS) was dispersed again in deionized water (400 mL) and placed in a sonication bath for 2 h with strong stirring. Then the L-GNS dispersion was gradually added into a $FeCl_3$ solution, in which 10 g $FeCl_3$ was dissolved in 500 mL deionized water in a 1000 mL three-necked flask. Similarly, a sufficient and violent stir for 6 h was handled to guarantee the complete complexation between iron ion and sodium lignosulfonate. The final product was collected by vacuum filtration and rinsed drastically with DMF. The obtained product was dried in a vacuum at 80 °C for 2 days to remove the residual solvent. Figure 1 illustrates the overall functionalization of graphene (FGNS).

2.4. Preparation of TPU/FGNS Composites. TPU was dried in an oven at 100 °C for 24 h in order to remove absorbed water. The TPU nanocomposites were fabricated by a co-coagulation plus compression molding technique. Briefly, 49.75 g of TPU was dissolved in 100 mL of DMF at 80 °C through a vigorous agitation for 2 h. FGNS (0.25 g) was dispersed in 100 mL DMF with ultrasonication to obtain the FGNS suspension. Following, the FGNS suspension was mixed with TPU solution under vigorous agitation. The mixture was then poured into 500 mL of deionized water under slight

DOI: 10.1021/acs.iecr.6b02579
Ind. Eng. Chem. Res. 2016, 55, 10681−10689

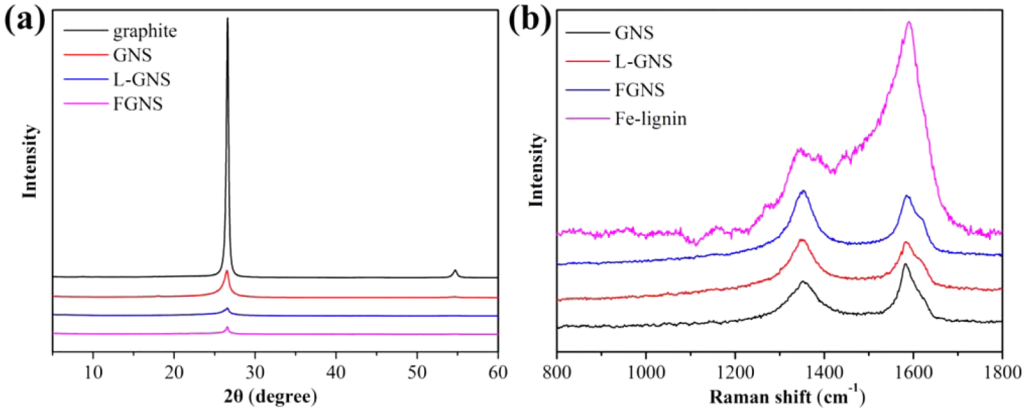

Figure 2. (a) XRD patterns of graphite, GNS, L-GNS, and FGNS; (b) Raman spectra of GNS, L-GNS, FGNS, and Fe-lignin.

stirring to obtain the flocculate of TPU/FGNS composites (TPU-0.5). The obtained flocculate was filtered and dried at 100 °C under oven for 24 h to remove adsorbed water. Other samples containing 1.0 and 2.0 wt% FGNS were produced by the same method. Finally, the sample was hot-pressed into sheets of appropriate size under 10 MPa at 190 °C for 10 min.

2.5. Measurements and Characterization. X-ray diffraction (XRD) measurements were recorded using a Japan Rigaku D/Max-Ra rotating anode X-ray diffractometer equipped with a CuK$_\alpha$ tube and Ni filter (λ= 0.1542 nm). The scope was 5−70° with a scan step of 4° min^{-1} scanning rate.

Fourier transform infrared spectroscopy (FTIR) signal was collected by a Nicolet 6700 spectrometer (Nicolet Instrument Company) in the 400−4000 cm^{-1} region to analyze sample with the transmission mode.

Raman spectroscopy was handled with a SPEX-1403 laser Raman spectrometer (SPEX Co., U.S.) with excitation provided in backscattering geometry by a 514.5 nm argon laser line.

Thermogravimetric analysis (TGA) was probed by the TGA Q5000 IR thermogravimetric analyzer (TA Instruments, U.S.) from 50 to 800 °C with a heating rate of 20 °C min^{-1} in nitrogen atmosphere.

Transmission electron microscopy (TEM) was performed through a JEOL JEM-2100F transmission electron microscope at an accelerating voltage of 200 kV.

Dynamic mechanical analysis (DMA) was carried out with a DMA Q800 instrument (TA Instruments Inc., U.S.) at a frequency of 10 Hz and a temperature range from −80 to 150 °C at a linear heating rate of 5 °C min^{-1}.

The measurements of tensile strength and elongation at break were carried out through a CMT4204 universal instrument (MTS Systems Co. Ltd., China) in accordance with the Chinese standard of GB 13022-91. All samples were manufactured into the dumbbell shape with a razor blade in 200 mm/min rate.

The thermal conductivity was measured using a hot-disk thermal analyzer (TC 3000E, Xia xi technology, China) at room temperature, adopting the transient plane source technique.

X-ray photoelectron spectroscopy (XPS) measurement was used to research the surface element of the hybrids, with a Kratos Axis Ultra DLD spectrometer employing a monochromatic Al K$_\alpha$ X-ray source ($h\nu$ = 1486.6 eV), hybrid (magnetic/electrostatic) optics, and a multichannel plate and delay line detector.

3. RESULTS AND DISCUSSION

3.1. Electrochemical Exfoliation and Noncovalent Functionalization. The XRD patterns were used to investigate the crystal structure of graphite, GNS, L-GNS, and FGNS. There is a remarkable difference between the XRD patterns (Figure 2a) of graphite and the others. A sharp peak at 26.6° indicating the interlayer spacing of graphite was greatly crippled in the other three curves. This phenomenon confirms that graphite was successfully exfoliated by electrochemical approach.[7] Among all of the curves, the reflection peak of GO (002) is unable to be found, indicating a weak oxidation degree of exfoliated graphene. The L-GNS and FGNS exhibit the weaker reflection peak than that of GNS, which is attributed to that iron lignosulfonate effectively adsorbed on the graphene surface and inhibited by the restack of graphene.

Raman spectroscopy was always performed to investigate the structure of carbonaceous materials. An argon laser line of 514.5 nm was applied, and samples were directly deposited on the quartz slice in the absence of solvents. Raman spectra of GNS, L-GNS, FGNS, and Fe-lignin are shown in Figure 2b. Two peaks located around 1355 and 1588 cm^{-1} could be observed in the fore three Raman spectra, which are called D band and G band, respectively.[22] The D band (around 1360 cm^{-1}) which originates from one breathing mode of k-point photons of A_{1g} symmetry is a defect-induced band and derived from the defective graphite structures. The G band (around 1600 cm^{-1}) originates from sp^2-bonded carbon atom in a 2D hexagonal lattice. In some literature, the relevant intensity ratio of D and G bands (I_D/I_G) is regarded as an effective measure to evaluate the disorder degree of carbon materials.[23] By comparing the I_D/I_G values of GNS (1.27), L-GNS (1.40), and FGNS (1.31), it can obviously be seen that the functionalization process did not overmuch destroy the structure of graphene sheets. In addition, the pronounced D peak is mainly due to the inevitable oxidation when exfoliation process was performed on anode. Considering the existence of sodium lignosulfonate, it is no wonder that L-GNS express higher I_D/I_G than GNS, because absorbed sodium lignosulfonate is likely regarded as defect of graphene. It is noteworthy that Fe-lignin exhibits two peaks located around 1338 and 1593 cm^{-1}. The band at 1593 cm^{-1} merged with G band (1588 cm^{-1}) to give higher intensity of G band for FGNS.[24] Therefore, the further modification of L-GNS with iron ion may cause a decrease in the I_D/I_G values for FGNS (1.31) from L-GNS (1.40).

DOI: 10.1021/acs.iecr.6b02579
Ind. Eng. Chem. Res. 2016, 55, 10681−10689

TEM measurement was used to characterize the morphologies of GNS, L-GNS, and FGNS. Figure 3a presents a typical

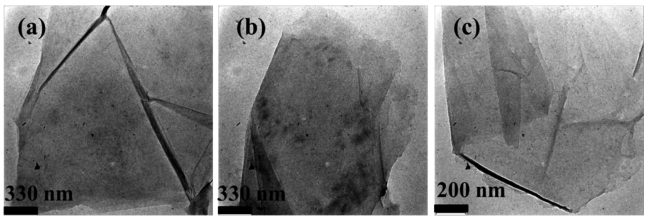

Figure 3. TEM images of (a) GNS, (b) L-GNS, and (c) FGNS.

TEM image of GNS, in which the graphene exhibits thin flaky and weak wrinkle morphologies. Compared to the RGO reported in previous article,[25] electrochemically exfoliated graphene shows less wrinkle in surface morphology. This phenomenon manifests that electrochemically exfoliated graphene possesses a more smooth surface and lower defect. Consistent with the previous study, electrochemically exfoliated graphene owns a large flake size with several micrometers in length due to mild experimental conditions (Figure 3).[7,26] Moreover, the absorbed Fe-lignin did not destroy the flaky morphology and large lateral size of graphene sheet during the process of surface functionalization.

FTIR measurement was carried out to confirm the successful modification of graphene, as presented in Figure 4a. The FTIR spectrum of GNS reveals some representative absorption peaks of oxygen-containing group: O−H stretching vibration (3433 cm^{-1}), C═C or H_2O vibration (1630 cm^{-1}). Compared to GNS, L-GNS and FGNS exhibit a new peak at 2922 cm^{-1}, which is attributed to the asymmetric vibration of alkyl group. The appearance of alkyl group indicates the stable absorption of ligninsulfonate on the surface of graphene. As for L-GNS, the peak at 1057 cm^{-1} can be assigned to the symmetric of the $-SO_3^-$ group.[27] In Figure 4, GNS and sodium lignosulfonate present a traditional broad υ_{O-H} at 3000−3600 cm^{-1}, centering at 3433 and 3432 cm^{-1}, respectively. However, it is obvious to find that red shift exists in the υ_{O-H} of L-GNS (3415 cm^{-1}). This phenomenon illustrates that sodium lignosulfonate combines with GNS via formation of hydrogen-bond action.[28,29] In addition, analogous red shifts can be observed at the bending vibration of Ar−H (from 773 to 758 cm^{-1}) and the C═C stretching of benzene ring (from 1599 to 1579 cm^{-1}). All of the results indicate the mechanism of sodium ligninsulfonate functionalized graphene is based on $\pi-\pi$ interaction and hydrogen bonding.[30] As might have been expected, the absorption peak that belonged to the $-SO_3^-$ group could not be found after complexing with iron. In addition, a new strong peak at 1082 cm^{-1} appears in the FTIR spectrum of FGNS. In general, when organic ligands combine with metal ion, the frequency and wavelength of chemical bond will obviously be changed.[31] It is thought that the variation of absorption peak of FGNS is attributed to the complexation between iron and lignosulfonate, which creates an intense dative bond. These results prove the successful combination between iron ion and lignosulfonate, as well as the attachment on the surface of graphene.

In order to further confirm the successful modification of GNS, XPS was performed to investigate the surface element characters of GNS, L-GNS, and FGNS (Figure 4b). The XPS data indicates the low oxidation of electrochemically exfoliated GNS, which only contains 12.33% of oxygen and is lower than that of RGO.[28] In contrast the new S 2p and Fe 2p peaks of absorbed Fe-lignin can be observed in the XPS spectrum of FGNS. The result also demonstrates the successful functionalization of GNS through noncovalent attachment and further complexation.

3.2. XRD Analysis of TPU/FGNS Nanocomposites.

Figure 5 presents the X-ray diffraction curves of pure TPU

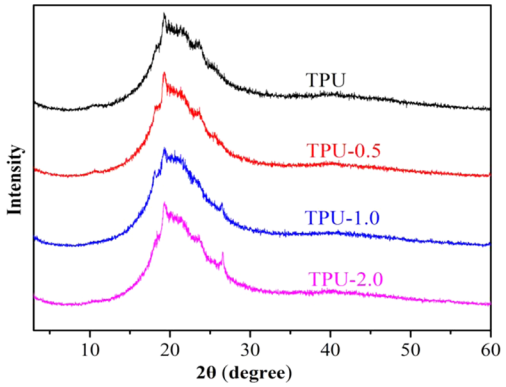

Figure 5. XRD patterns of TPU and nanocomposites.

and the TPU/FGNS nanocomposites. A broad peak at $2\theta \approx 19.4°$ can be observed in the curves of the pure TPU and TPU/FGNS nanocomposites. It illustrates the incorporation of FGNS does not obviously affect the crystallization performance of TPU. When the FGNS content was only 0.5 wt%, it was not found by the peak near 26.6°. Even though the concentration of FGNS receives 1.0 wt%, only a feeble peak can be caught in

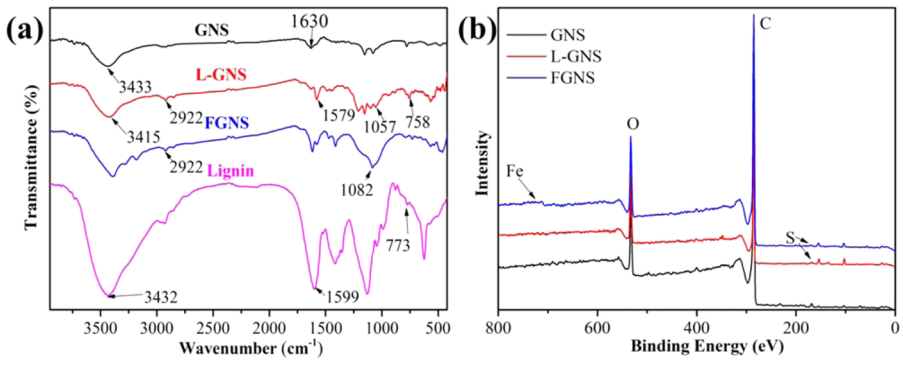

Figure 4. (a) FTIR spectra of GNS, L-GNS, and FGNS; (b) XPS survey scans of GNS, L-GNS, and FGNS.

DOI: 10.1021/acs.iecr.6b02579
Ind. Eng. Chem. Res. 2016, 55, 10681−10689

26.6°. This confirms a good dispersion of FGNS in TPU matrix at low FGNS content. For TPU-2.0, high content of FGNS and large specific surface area lead to partial stack of FGNS. The phenomenon is consistent with previous reports.[32]

3.3. Mechanical Behavior of TPU/FGNS Nanocomposites. The interfacial interaction of nanofiller in polymer matrix plays a vital factor to improve various performances of polymer nanocomposite, especially in mechanical property. SEM was carried out to investigate the fracture morphologies of TPU/FGNS nanocomposites and evaluate the interfacial interaction. It is obviously found that pure TPU exhibits a smooth and flat cross section (Figure 6a and d), indicating a typical brittle failure. When FGNS was introduced into polymer matrix, the fracture surfaces of TPU composite became rough and uneven, indicating the strong interfacial adhesion between FGNS and TPU matrix. As revealed in Figure 6c and f, visible agglomerates could not be observed.

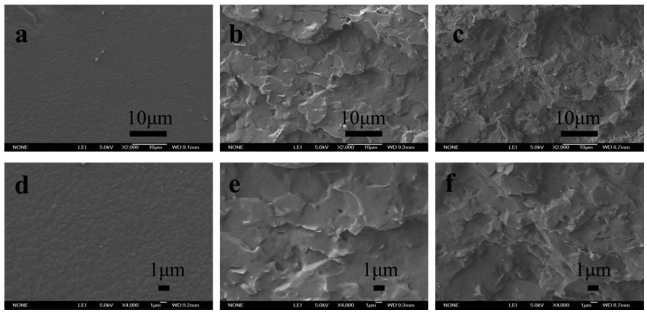

Figure 6. SEM images of the fractured surfaces of (a and d) TPU, (b and e) TPU-1.0, and (c and f) TPU-2.0.

Due to the strong interfacial interaction, efficient load transfer from weak polymer chains to robust graphene can obviously improve the mechanical properties of TPU nanocomposites. The tensile test (Figure 7a) was carried to investigate the reinforcement of FGNS on the mechanical properties of TPU nanocomposites. According to the stress−strain plots of TPU and its nanocomposites, introduced FGNS can obviously improve the tensile strain when maintaining a considerable elongation. It owes to the organic portion of Fe-lignin that enhances the load delivery to the robust inorganic filler with improved interface interaction. The high two-dimensional sheet concentration breaks the tangle of polymer chain and causes continuous cracks, decreasing the mechanical properties of polymer.[33] Therefore, increasing FGNS content leads to simultaneous decrease in both tensile strength and strain at break. Besides, Figure 7b displays the storage modulus of neat TPU and TPU-2.0. The storage modulus of TPU-2.0 exhibits a significant improvement in all the temperature ranges compared to that of pure TPU. It indicates that incorporating FGNS restrains the movement of chain segment on account of the nature of FGNS and the enhanced interface interaction between nanofiller and TPU matrix.

3.4. Thermal Properties of TPU/FGNS Nanocomposites. TGA is a universal equipment to assess the thermal stability of TPU and its composites. In Table 1, a negligible disparity about the 5% weight loss temperature ($T_{-5\%}$) of TPU nanocomposites is found, indicating the incorporation of FGNS did not change the initial degradation process of TPU. As Figure 8a and Table 1 stated, adding FGNS can obviously increase the char residues of TPU nanocomposites, which is triple over that of pure TPU when 2.0 wt% FGNS is incorporated. It is attributed to the protective char particles derived from Fe-lignin covered on the surface of graphene, thus forming the graphene based char layer with an intact lamella. The thermal conductivity of TPU nanocomposites was improved by introducing FGNS and the degree of enhancement depends on the contents of FGNS (Figure 8b). The thermal conductivity of TPU-0.5 was clearly increased compared to that of pure TPU. The TPU-2.0 exhibits the highest enhancement on thermal conductivity. According to previous report,[34] the thermal conductivity of polymer nanocomposites depends on the dispersion degree and intrinsic property of graphene. In this case, the well-dispersion and inherent high thermal conductivity of FGNS are the two key points to result in the dramatic enhancement on thermal conductivity.

Table 1. TGA Data of TPU Nanocomposites in Nitrogen Atmosphere

sample	$T_{-5\%}$ (°C)	T_{max1} (°C)	T_{max2} (°C)	char residue at 700 °C (wt%)
TPU	287	300	399	3.6
TPU-0.5	289	309	402	4.2
TPU-1.0	285	322	378	5.9
TPU-2.0	286	327	371	9.4

3.5. Flame Retardancy of TPU/FGNS Nanocomposites and Char Residues after Cone Calorimeter. The flammability of polymers were evaluated by cone calorimeter, which is a universal and effective tool in investigating the combustion behavior. Heat release rate (HRR) and total heat release (THR) curves of TPU and its composites are depicted

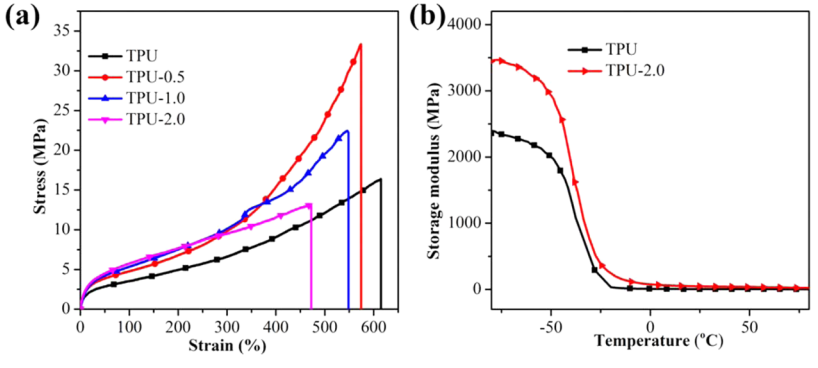

Figure 7. (a) Stress−strain curves of TPU and nanocomposites and (b) storage modulus of TPU and TPU-2.0.

DOI: 10.1021/acs.iecr.6b02579
Ind. Eng. Chem. Res. 2016, 55, 10681−10689

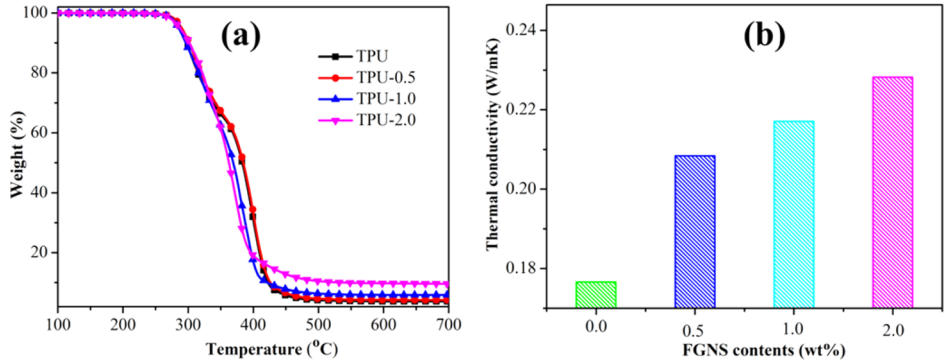

Figure 8. (a) TG curves of TPU and its composites under nitrogen atmosphere. (b) Thermal conductivity plot of TPU nanocomposites at different contents.

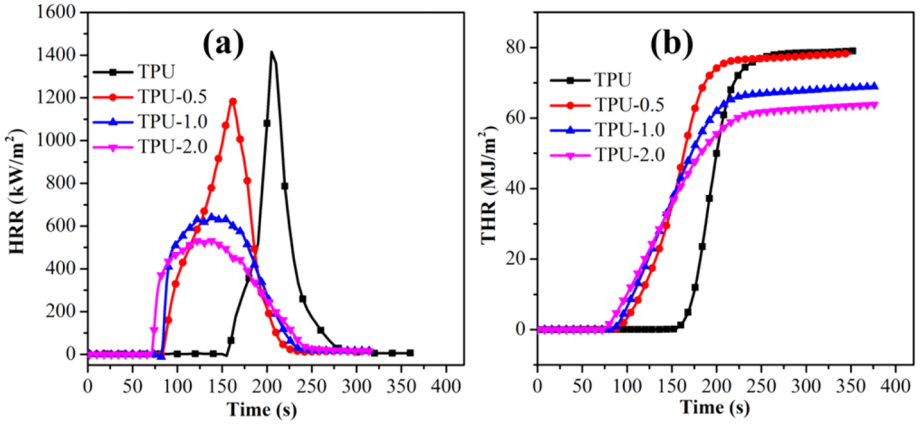

Figure 9. (a) HRR and (b) THR vs time curves of TPU and its composites.

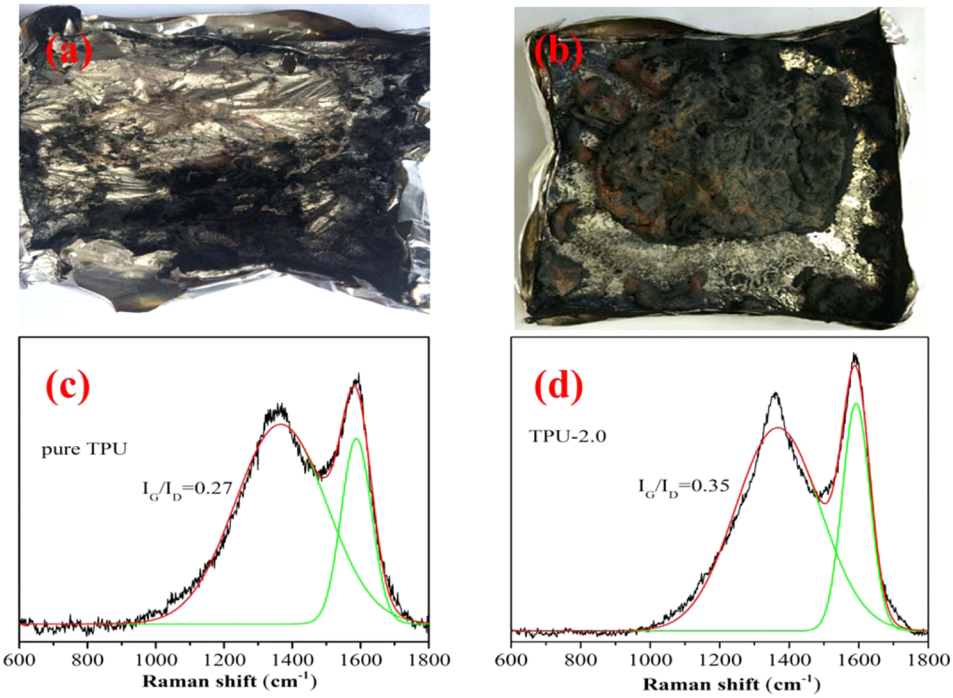

Figure 10. Digital photographs of the char residue of (a) TPU and (b) TPU-2.0 after cone calorimetry test. Raman spectra of the char residues of (c) TPU and (d) TPU-2.0.

in Figure 9. It could be found that the neat TPU burned violently with a sharp HRR peak (1408 kW m^{-2}). Evidently, compared to pure TPU, the pHRR value of TPU nanocomposites gradually decreased with increasing the contents of FGNS (Figure 9a). Through adding 2.0 wt% FGNS, pHRR decreased by more than half of the original level (from 1408 to

DOI: 10.1021/acs.iecr.6b02579
Ind. Eng. Chem. Res. 2016, 55, 10681−10689

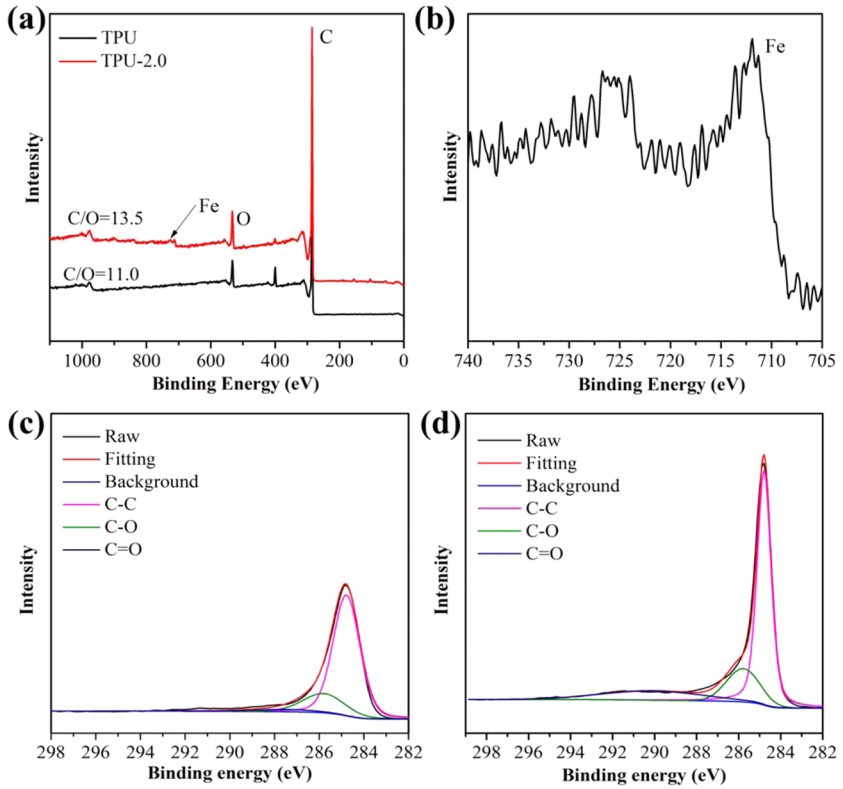

Figure 11. (a) XPS spectra of the char residues of TPU and TPU-2.0 after cone calorimetry test; (b) XPS spectra of Fe 2p. High-resolution C 1s XPS spectra of the char residues of (c) TPU and (d) TPU-2.0 after cone calorimetry test.

523 kW m^{-2}). Moreover, from Figure 9b, the THR of TPU-2.0 (78.6 MJ m^{-2}) was considerably reduced compared to pure TPU (63.9 MJ m^{-2}). Benefited from the catalytic carbonization of Fe-lignin, in situ formed char on the surface of graphene prevents the lamella structure of FGNS from overburning and thus forms the protective char layer. This stable char layer effectively hinders the delivery of degradation production with shield effect, thus imparting the excellent flame retardancy to TPU materials. As reported in previous literature,[35] graphene-based flame retardants usually decreased the ignition time. Obviously, it is attributed to the enhanced thermal conductivity, which facilitates the delivery of heat from the surface into the interior of TPU matrix.[36]

Figure 10 shows digital photographs of the residual char of TPU and TPU-2.0 after cone calorimetry test. Obviously, pure TPU was almost completely combusted, leaving threadlike char (Figure 10a). After introducing FGNS, residual char was clearly increased and it created a continuous extensive carbon layer (Figure 10b). Raman spectroscopy is a key tool to characterize carbonaceous materials. The structure of char residues indicates vital message regarding the flame retardant mechanism. Figure 10c and d present the Raman spectra of the char residues of TPU and TPU-2.0. Two remarkable peaks at 1373 and 1590 cm^{-1} are seized in the two spectra, relating to D and G bands. Generally, the proportion of the relevant intensity of G to D peak (I_G/I_D) is used to estimate the graphitization degree of the residual char.[23] The I_G/I_D of the char of TPU-2.0 (0.35) is obviously higher than that of the pure TPU (0.27). In terms, the addition of FGNS facilitates formation of high graphitized residue char with the shield effect, which is able to prevent the transfer of volatile by a more stable structure.

With the purpose of investigating the effect of FGNS, the element characters of residual char were studied by XPS. As Figure 11a indicates, iron exists in the remaining char and the peak at 711 eV can be assigned to the iron trioxide.[37] During the conversion from organic-iron complex to iron oxide, iron catches free radical from polymer matrix and plays a catalytic cross-linking effect to enhance the compactness of char.[37] Compared to neat TPU, the C/O atomic ratio is increased from 11.0 to 13.5 for the residual char of TPU-2.0, indicating the enhanced carbonization degree. The intensity of peak responding to the C 1s in the residual char of TPU-2.0 is higher obviously than that of pure TPU (Figure 11c and d). This phenomenon is in good agreement with above results and further verifies that the addition of FGNS can reduce the fire hazards of TPU nanocomposites by enhancing carbonization performance.

4. CONCLUSIONS

In this article, high quality and low defect graphene was prepared by an environmentally friendly and high yield electrochemical exfoliation route. Then the graphene was successfully modified through $\pi-\pi$ interaction and complexing action, which was confirmed by multiple tests (Raman spectra, FTIR, and XPS). Further, the TPU/FGNS nanocomposites were fabricated with a combination of co-coagulation and the compression molding technique. The incorporation of FGNS enhanced the thermal stability and thermal conductivity of TPU nanocomposite, due to the proper surface modification and intrinsic excellent performance of FGNS. Compared to pure TPU, the heat release rate was obviously inhibited (decline 63%) and the mechanical properties were significantly improved. The mechanism for these improvements was clearly

DOI: 10.1021/acs.iecr.6b02579
Ind. Eng. Chem. Res. 2016, 55, 10681−10689

interpreted. During combustion, the catalytic charring action of iron lignosulfonate together with the physical barrier effect of graphene sheets can form a protective char layer to restrain the transfer of flammable pyrolysis volatiles, thus improve the flame retardant property of TPU/FGNS nanocomposites. The reinforced mechanical behaviors of TPU nanocomposites was attributed to the bridging effect of lignin molecules, which can improve the load transfer efficiency with enhanced interaction between FGNS and TPU matrix.

AUTHOR INFORMATION

Corresponding Authors

*E-mail: yuanhu@ustc.edu.cn; Fax: +86-551-63601664; Tel: +86-551-63601664.

*E-mail: gongxl@ustc.edu.cn; Fax: +86-0551-63600419; Tel: +86-551-63600419.

Notes

The authors declare no competing financial interest.

ACKNOWLEDGMENTS

The research grants were supported by the National Natural Science Foundation of China (grant nos. 21374111 and 51323010) and the Fundamental Research Funds for the Central Universities (grant nos. WK2320000032).

REFERENCES

(1) Hu, Y.; Guan, C.; Feng, G.; Ke, Q.; Huang, X.; Wang, J. Flexible Asymmetric Supercapacitor Based on Structure-Optimized Mn_3O_4/Reduced Graphene Oxide Nanohybrid Paper with High Energy and Power Density. *Adv. Funct. Mater.* **2015**, *25*, 7291.

(2) Alizadeh, T.; Azizi, S. Graphene/graphite paste electrode incorporated with molecularly imprinted polymer nanoparticles as a novel sensor for differential pulse voltammetry determination of fluoxetine. *Biosens. Bioelectron.* **2016**, *81*, 198.

(3) Li, Y. L.; Zhang, Z. Q.; Pei, L. Y.; Li, X. G.; Fan, T.; Ji, J.; Shen, J. F.; Ye, M. X. Multifunctional photocatalytic performances of recyclable Pd-$NiFe_2O_4$/reduced graphene oxide nanocomposites via different co-catalyst strategy. *Appl. Catal., B* **2016**, *190*, 1.

(4) Feng, X.; Xing, W.; Song, L.; Hu, Y.; Liew, K. M. TiO_2 loaded on graphene nanosheet as reinforcer and its effect on the thermal behaviors of poly(vinyl chloride) composites. *Chem. Eng. J.* **2015**, *260*, 524.

(5) Aneja, K. S.; Bohm, S.; Khanna, A. S.; Bohm, H. L. M. Graphene based anticorrosive coatings for Cr(VI) replacement. *Nanoscale* **2015**, *7*, 17879.

(6) Zhong, Y. L.; Tian, Z. M.; Simon, G. P.; Li, D. Scalable production of graphene via wet chemistry: progress and challenges. *Mater. Today* **2015**, *18*, 73.

(7) Parvez, K.; Wu, Z. S.; Li, R. J.; Liu, X. J.; Graf, R.; Feng, X. L.; Mullen, K. Exfoliation of Graphite into Graphene in Aqueous Solutions of Inorganic Salts. *J. Am. Chem. Soc.* **2014**, *136*, 6083.

(8) Yang, S.; Bruller, S.; Wu, Z. S.; Liu, Z. Y.; Parvez, K.; Dong, R. H.; Richard, F.; Samori, P.; Feng, X. L.; Mullen, K. Organic Radical-Assisted Electrochemical Exfoliation for the Scalable Production of High-Quality Graphene. *J. Am. Chem. Soc.* **2015**, *137*, 13927.

(9) Wang, J. Y.; Huang, J. L.; Yan, R.; Wang, F. X.; Cheng, W. G.; Guo, Q. G.; Wang, J. Z. Graphene microsheets from natural microcrystalline graphite minerals: scalable synthesis and unusual energy storage. *J. Mater. Chem. A* **2015**, *3*, 3144.

(10) Liu, J. L.; Poh, C. K.; Zhan, D.; Lai, L. F.; Lim, S. H.; Wang, L.; Liu, X. X.; Gopal Sahoo, N.; Li, C. M.; Shen, Z. X.; Lin, J. Y. Improved synthesis of graphene flakes from the multiple electrochemical exfoliation of graphite rod. *Nano Energy* **2013**, *2*, 377.

(11) John, B.; Motokucho, S.; Kojio, K.; Furukawa, M. Polyamide 6 Fibers with Superior Mechanical Properties: TPU Coating Techniques. *Sen'i Gakkaishi* **2009**, *65*, 236.

(12) Xiang, C. S.; Lu, W.; Zhu, Y.; Sun, Z. Z.; Yan, Z.; Hwang, C. C.; Tour, J. M. Carbon Nanotube and Graphene Nanoribbon-Coated Conductive Kevlar Fibers. *ACS Appl. Mater. Interfaces* **2012**, *4*, 131.

(13) Yang, L. P.; Phua, S. L.; Toh, C. L.; Zhang, L. Y.; Ling, H.; Chang, M. C.; Zhou, D.; Dong, Y. L.; Lu, X. H. Polydopamine-coated graphene as multifunctional nanofillers in polyurethane. *RSC Adv.* **2013**, *3*, 6377.

(14) Amir, A.; Mahalingam, S.; Wu, X.; Porwal, H.; Colombo, P.; Reece, M. J.; Edirisinghe, M. Graphene nanoplatelets loaded polyurethane and phenolic resin fibres by combination of pressure and gyration. *Compos. Sci. Technol.* **2016**, *129*, 173.

(15) Yang, W.; Yang, B. H.; Lu, H. D.; Song, L.; Hu, Y. Effect of Modified Carbon Nanotube on the Thermal Behavior, Flame Retardancy and Mechanical Properties of Poly(1,4-butylene terephthalate)/Aluminum Phosphinate Composites. *Ind. Eng. Chem. Res.* **2014**, *53*, 18489.

(16) Lin, M.; Li, B.; Li, Q. F.; Li, S.; Zhang, S. Q. Synergistic Effect of Metal Oxides on the Flame Retardancy and Thermal Degradation of Novel Intumescent Flame-Retardant Thermoplastic Polyurethanes. *J. Appl. Polym. Sci.* **2011**, *121*, 1951.

(17) Wu, X.; Mahalingam, S.; Amir, A.; Porwal, H.; Reece, M. J.; Naglieri, V.; Colombo, P.; Edirisinghe, M. Novel Preparation, Microstructure, and Properties of Polyacrylonitrile-Based Carbon Nanofiber−Graphene Nanoplatelet Materials. *ACS Omega* **2016**, *1*, 202.

(18) Yuan, B.; Sheng, H.; Mu, X.; Song, L.; Tai, Q.; Shi, Y.; Liew, K. M.; Hu, Y. Enhanced flame retardancy of polypropylene by melamine-modified graphene oxide. *J. Mater. Sci.* **2015**, *50*, 5389.

(19) Feng, X. M.; Wang, X.; Xing, W. Y.; Yu, B.; Song, L.; Hu, Y. Simultaneous Reduction and Surface Functionalization of Graphene Oxide by Chitosan and Their Synergistic Reinforcing Effects in PVA Films. *Ind. Eng. Chem. Res.* **2013**, *52*, 12906.

(20) Bao, C.; Guo, Y.; Yuan, B.; Hu, Y.; Song, L. Functionalized graphene oxide for fire safety applications of polymers: a combination of condensed phase flame retardant strategies. *J. Mater. Chem.* **2012**, *22*, 23057.

(21) Ferrari, A. C.; Meyer, J. C.; Scardaci, V.; Casiraghi, C.; Lazzeri, M.; Mauri, F.; Piscanec, S.; Jiang, D.; Novoselov, K. S.; Roth, S.; Geim, A. K. Raman spectrum of graphene and graphene layers. *Phys. Rev. Lett.* **2006**, *97*, 187401.

(22) Yang, S.; Yue, W. B.; Huang, D. Z.; Chen, C. F.; Lin, H.; Yang, X. J. A facile green strategy for rapid reduction of graphene oxide by metallic zinc. *RSC Adv.* **2012**, *2*, 8827.

(23) Amarnath, C. A.; Hong, C. E.; Kim, N. H.; Ku, B. C.; Kuila, T.; Lee, J. H. Efficient synthesis of graphene sheets using pyrrole as a reducing agent. *Carbon* **2011**, *49*, 3497.

(24) Zhou, K.; Gui, Z.; Hu, Y. The influence of graphene based smoke suppression agents on reduced fire hazards of polystyrene composites. *Composites, Part A* **2016**, *80*, 217.

(25) Munuera, J. M.; Paredes, J. I.; Villar-Rodil, S.; Ayan-Varela, M.; Martinez-Alonso, A.; Tascon, J. M. D. Electrolytic exfoliation of graphite in water with multifunctional electrolytes: en route towards high quality, oxide-free graphene flakes. *Nanoscale* **2016**, *8*, 2982.

(26) Jiang, Z. Q.; Zhao, X. S.; Fu, Y. Z.; Manthiram, A. Composite membranes based on sulfonated poly(ether ether ketone) and SDBS-adsorbed graphene oxide for direct methanol fuel cells. *J. Mater. Chem.* **2012**, *22*, 24862.

(27) Bao, C. L.; Guo, Y. Q.; Song, L.; Hu, Y. Poly(vinyl alcohol) nanocomposites based on graphene and graphite oxide: a comparative investigation of property and mechanism. *J. Mater. Chem.* **2011**, *21*, 13942.

(28) Song, P. a.; Xu, Z.; Lu, Y.; Guo, Q. Bioinspired strategy for tuning thermal stability of PVA via hydrogen-bond crosslink. *Compos. Sci. Technol.* **2015**, *118*, 16.

(29) Pei, Z. G.; Li, L. Y.; Sun, L. X.; Zhang, S. Z.; Shan, X. Q.; Yang, S.; Wen, B. Adsorption characteristics of 1,2,4-trichlorobenzene, 2,4,6-trichlorophenol, 2-naphthol and naphthalene on graphene and graphene oxide. *Carbon* **2013**, *51*, 156.

DOI: 10.1021/acs.iecr.6b02579
Ind. Eng. Chem. Res. 2016, 55, 10681−10689

(30) Finnegan, M. M.; Lutz, T. G.; Nelson, W. O.; Smith, A.; Orvig, C. Neutral Water-Soluble Post-Transition-Metal Chelate Complexes of Medical Interest - Aluminum and Gallium Tris(3-Hydroxy-4-Pyronates). *Inorg. Chem.* **1987**, *26*, 2171.
(31) Liu, S.; Yan, H. Q.; Fang, Z. P.; Wang, H. Effect of graphene nanosheets on morphology, thermal stability and flame retardancy of epoxy resin. *Compos. Sci. Technol.* **2014**, *90*, 40.
(32) Bao, C.; Zhang, H.; Wilkie, C. A.; Bi, S.; Tang, X.-Z.; Wu, J.; Yang, J. On the dispersion systems of graphene-like two-dimensional materials: From fundamental laws to engineering guidelines. *Carbon* **2016**, *107*, 774.
(33) Yang, L.; Phua, S. L.; Toh, C. L.; Zhang, L.; Ling, H.; Chang, M.; Zhou, D.; Dong, Y.; Lu, X. Polydopamine-coated graphene as multifunctional nanofillers in polyurethane. *RSC Adv.* **2013**, *3*, 6377.
(34) Bao, C. L.; Song, L.; Wilkie, C. A.; Yuan, B. H.; Guo, Y. Q.; Hu, Y.; Gong, X. L. Graphite oxide, graphene, and metal-loaded graphene for fire safety applications of polystyrene. *J. Mater. Chem.* **2012**, *22*, 16399.
(35) Qian, X.; Song, L.; Yu, B.; Wang, B.; Yuan, B.; Shi, Y.; Hu, Y.; Yuen, R. K. K. Novel organic-inorganic flame retardants containing exfoliated graphene: preparation and their performance on the flame retardancy of epoxy resins. *J. Mater. Chem. A* **2013**, *1*, 6822.
(36) Kamiya, K.; Hashimoto, K.; Nakanishi, S. Instantaneous one-pot synthesis of Fe-N-modified graphene as an efficient electrocatalyst for the oxygen reduction reaction in acidic solutions. *Chem. Commun.* **2012**, *48*, 10213.
(37) Jang, J.; Kim, J.; Bae, J. Y. Effects of Lewis acid-type transition metal chloride additives on the thermal degradation of ABS. *Polym. Degrad. Stab.* **2005**, *88*, 324.

DOI: 10.1021/acs.iecr.6b02579
Ind. Eng. Chem. Res. 2016, 55, 10681−10689